Journal of Scientific Computing, Vol. 28, Nos. 2/3, September 2006 (© 2006)
DOI: 10.1007/s10915-006-9080-1

A Boundary Integral Equation Method for Photonic Crystal Fibers

Min Hyung Cho,[1,†] Wei Cai,[1,2] and Tsing-Hua Her[2,3]

Received April 7, 2005; accepted (in revised form) September 20, 2005; Published online March 13, 2006

A boundary integral equation for the eigenmode of photonic crystal fibers is formulated and numerically solved using the Nyström method. The real and imaginary parts of the propagation constant, which are related to the dispersion and the confinement loss of fibers, are obtained using a secant method. This formulation is very flexible to handle the fiber geometry, and therefore can be applied to photonic crystal fibers with novel refractive index profile and hole geometry.

KEY WORDS: Boundary integral equations; Helmholtz equation; photonic crystal fibers; photonic crystal.

1. INTRODUCTION

Photonic crystal fibers (PCF) consist of a periodic array of holes running through the length of the fibers with defects in the lattice, which serve as cores for light guiding. When the average refractive index in the cladding is lower than that of the core, light is guided based on total internal reflection [3]; whereas when the refractive index in the cladding is higher than that of the core, light is guided based on constructive interference [8]. Thanks to its novel guiding mechanisms, which render a pyramid of interesting properties and exciting potential applications, PCF has become one of the most exciting topics in fiber optics [11, 14].

[†]Support for this work is partially provided by the National Science Foundation Grant DMS-0408309 and the Department of Energy Grant DE-FG02-05ER25678.

[1]Department of Mathematics and Statistics, University of North Carolina at Charlotte, Charlotte, NC 28223, USA. E-mail: wcai@uncc.edu
[2]Department of Physics and Optical Science, University of North Carolina at Charlotte, Charlotte, NC 28223, USA.
[3]Center for Optoelectronics and Optical Communications, Charlotte, NC 28223, USA.

Many simulation methods have been applied to study PCF, including the beam propagation method [1, 12], the multipole method [18, 19], the scattering matrix method [10] and the finite element method (FEM) [15]. In this paper, we propose to study the guiding properties of PCF using a boundary integral equation (BIE), which based on Huygen's principal and Green's function. There are advantages of using BIE compared to other methods: FEM requires discretization of the interior domain and truncation of the exterior domain with triangular or rectangular elements, while the multipole method is restricted to perfect circular domains. On the other hand, BIE uses only the boundary, and therefore it can handle almost arbitrary shapes and distribution of holes with a smaller number of unknowns. Because a boundary condition at infinity is built into the Green's function, the Perfect Matching Layer [15] or the Artificial Boundary Condition is not needed for the truncation of solution domains for the BIE method. Another advantage of the BIE is that it can handle arbitrary profiles of the refractive index of holes, which can be used to simulate the tunability of PCF easily.

However, discretization of the integral operators in the BIE method yields a full matrix, and the mode searching step is somewhat time consuming. The latter issue has been studied by Xiaoyan Wang *et al.* [17]. In their approach, the Helmholtz equation is considered as a Poisson equation with a solution dependent body force term. This allows them to separate the wave number k from Green's function, which reduces significantly the mode searching time. However, because Green's function is a natural logarithm function, their method can only handle the real part of the propagation constant. The BIE method, on the other hand, can yield both the real and imaginary parts of the propagation constant, thus providing more complete information for modeling PCF.

The paper is organized as follows: In Section 2, the BIE is derived from the Maxwell's equation, and some numerical issues are stated in Section 3. In Section 4, we apply the BIE method to obtain the propagation characteristics of two types of PCFs to demonstrate the validity of this method. Finally, Section 5 summarizes the current work and lays out the future direction of our research.

2. FORMULATION

The governing equation for PCF is the Maxwell's equations. By assuming time harmonic $\exp(-i\omega t)$ and z dependence $\exp(i\beta z)$ along the fiber, the Maxwell's equations can be reduced to a Helmholtz equation with unknown complex propagation constant β, namely

$$\left(\frac{\partial^2}{\partial x^2}+\frac{\partial^2}{\partial y^2}\right)\psi+k_j^2\psi=0 \tag{1}$$

$$\lim_{r\to\infty}\sqrt{r}\left(\frac{\partial\psi}{\partial r}-ik_1\psi\right)=0, \tag{2}$$

where

$$k_j=\sqrt{k_0^2n_j^2-\beta^2}, \quad j=1,2 \tag{3}$$

and $k_0=2\pi/\lambda$ is the wave number in vacuum, $j=1$ denotes the exterior of collection of holes and $j=2$ denotes the interior of holes. The z-dependence in the assumption can be expanded out as

$$\exp(i\beta z)=\exp(i(\alpha_1+i\alpha_2)z)=\exp(i\alpha_1 z)\exp(-\alpha_2 z). \tag{4}$$

Then, $\mathrm{Re}(\beta)=\alpha_1$ gives the propagation constant of the light along the fiber and $\mathrm{Im}(\beta)=\alpha_2>0$ gives the decay rate or the confinement loss of the light. In the following, by using the Green's function for the Helmholtz equation and Green's second identity, a BIE will be formulated for the interior domain D_j and the exterior domain $R^2\setminus\cup_{j=1}^{N}D_j$ of the fiber shown in Fig. 1.

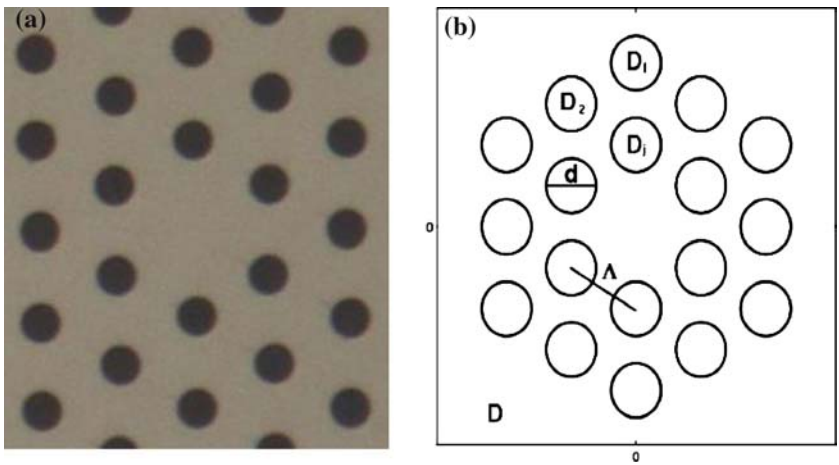

Fig. 1. Photonic crystal fiber (a) optical image of portion of the cross section of a PCF with empty holes. (b) Domain with notation. d denotes diameter of holes, Λ denotes the distance between holes, D_j denotes the interior of jth hole, and D denotes exterior domain.

2.1. Interior Domain

For any $\hat{r} \in D_j$, both solution ψ and Green's function $G_j(\hat{r}-r) = \frac{i}{4}H_0^{(1)}(k_2 \mid \hat{r}-r \mid)$ satisfy the Helmholtz equation with zero and $-\delta(\hat{r}-r)$ right hand side, respectively

$$\Delta\psi(\hat{r}) + k_2^2\psi(\hat{r}) = 0, \tag{5}$$

$$\Delta G_j(\hat{r}-r) + k_2^2 G_j(\hat{r}-r) = -\delta(\hat{r}-r). \tag{6}$$

Subtracting (6) $\times\psi(r)$ from (5) $\times G_j(\hat{r}-r)$ and integrating over the domain D_j yield

$$\psi(\hat{r}) = \int_{D_j} G_j(\hat{r}-r)\Delta\psi(r)\ dr - \int_{D_j} \Delta G_j(\hat{r}-r)\psi(r)\ dr. \tag{7}$$

Then, using Green's second identity, (7) can be converted into boundary integrals, namely

$$\psi(\hat{r}) = \int_{\partial D_j} G_j(\hat{r}-r)\frac{\partial\psi}{\partial n}(r)\ ds(r) - \int_{\partial D_j} \frac{\partial G_j}{\partial n}(\hat{r}-r)\psi(r)\ ds(r). \tag{8}$$

Because the solutions on the boundary are used to express the field away the boundary, this representation can be regarded as Huygens principal. This formula will be used to calculate the field points inside domain D_j after solving the BIE. In order to arrive at the BIE, we will let $\hat{r}$ approach to r on the interface. For the term involve G_j itself, we can pass the limit inside. However, the term $\partial G_j/\partial n$ will produce a singular contribution of $-\frac{1}{2}\psi(\hat{r})$ due to Plemelj formula [13, 16]. Then, we have

$$\psi(\hat{r}) = \int_{\partial D_j} G_j(\hat{r}-r)\frac{\partial\psi}{\partial n}\ ds(r) + \frac{1}{2}\psi(\hat{r}) - \int_{\partial D_j} \frac{\partial G_j}{\partial n}(\hat{r}-r)\psi(r)\ ds(r) \tag{9}$$

and moving all the terms to the left hand side and multiplying by a factor of two yield the BIE for the interior domain

$$\psi(\hat{r}) + 2\int_{\partial D_j} \frac{\partial G_j}{\partial n}(\hat{r}-r)\psi(r)\ ds(r) - \int_{\partial D_j} G_j(\hat{r}-r)\frac{\partial\psi}{\partial n}\ ds(r) = 0. \tag{10}$$

2.2. Exterior Domain

The formulation for the exterior domain is similar to the interior domain case with two slight differences. The first difference is that when applying Green's second identity, the boundary will involve infinity. But,

due to Sommerfeld radiation condition (2), the integral that involves the infinity boundary will converge to zero. Thus, Green's second identity can be applied without any difficulty. The second difference is that when we let $\hat{r}$ approach to r on the boundary, the normal derivative term produces $\frac{1}{2}\psi(\hat{r})$. Now for $\hat{r} \in R^2 \backslash D$, we can derive the BIE from

$$\psi(\hat{r}) = \int_{R^2 \backslash D} G(\hat{r} - r) \Delta\psi(r)\ dr - \int_{R^2 \backslash D} \Delta G(\hat{r} - r)\psi(r)\ dr. \tag{11}$$

Then, again Green's second identity yields

$$\psi(\hat{r}) = -\int_{\partial D} G(\hat{r} - r) \frac{\partial \psi}{\partial n}\ ds(r) + \int_{\partial D} \frac{\partial G}{\partial n}(\hat{r} - r)\psi(r)\ ds(r), \tag{12}$$

where $G(\hat{r} - r) = \frac{i}{4} H_0^{(1)}(k_1 |\hat{r} - r|)$, $D = \cup_{j=1}^{N} D_j$, and $\partial D = \cup_{i=1}^{N} \partial D_j$. Signs are changed due to the direction of normal vectors, which points toward the exterior domain. Finally, by letting $\hat{r}$ go to r on the boundary, we have

$$\psi(\hat{r}) - 2\int_{\partial D} \frac{\partial G}{\partial n}(\hat{r} - r)\psi(r)\ ds(r) + 2\int_{\partial D} G(\hat{r} - r) \frac{\partial \psi}{\partial n}\ ds(r) = 0. \tag{13}$$

2.3. Summary of Integral Operators

The integral with normal derivative of the Green's function is called a double layer potential and will be denoted as D while the integral with Green's function itself is called a single layer potential and will be denoted as S.

$$Su = \int_{\partial D} G(\hat{r} - r)u(r)\ ds(r), \tag{14}$$

$$Du = \int_{\partial D} \frac{\partial G}{\partial n}(\hat{r} - r)u(r)\ ds(r), \tag{15}$$

$$S_j u = \int_{\partial D_j} G_j(\hat{r} - r)u(r)\ ds(r), \tag{16}$$

$$D_j u = \int_{\partial D_j} \frac{\partial G_j}{\partial n}(\hat{r} - r)u(r)\ ds(r). \tag{17}$$

Then, using integral operator notation, Eqs. (10) and (13) can be rewritten in a matrix form

$$A(\beta)x = 0, \tag{18}$$

where

$$A(\beta)=\begin{pmatrix} I-2D & 2S \\ I+2D_j & -2S_j \end{pmatrix}, \quad x=\begin{pmatrix} u \\ \frac{\partial u}{\partial n} \end{pmatrix}. \tag{19}$$

Since the kernels of the integral operators contain the unknown β, matrix A is a function of β and a nontrivial solution of the Eq. (18), which can be found by solving $f(\beta)=|det(A(\beta))|=0$, will determine the eigenmode of PCF. For the purpose of complex root searching, the secant method is employed and each integral operator in the matrix is discretized using Nyström method [6]. After β is found, matrix equation can be solved to find solution on the boundary. Then, using the solution, the field points at everywhere can be calculated using Eqs. (8) and (12).

3. NUMERICAL METHOD

In this section, the Nyström or quadrature method for the single and double layer operators and mode searching method are presented. The Nyström method starts by applying straightforward quadrature method for the integral operators. As a consequence, all the matrix elements are simple evaluations of Green's function at the quadrature points. However, the Galerkin type and collocation methods use simple or double integrals as their matrix elements. Also the Nyström method is generally stable. But, in the case of other methods, condition numbers could be disturbed by a poor choice of the basis function [6].

3.1. Single Layer Potential (S)

As all the domains are circles with a radius a, we can let $x(t)=(a\cos t, a\sin t)$, $0\leqslant t\leqslant 2\pi$ be the parametric representation of the circle. With $G(\hat{r}-r)=\frac{i}{4}H_0^{(1)}(k|\hat{r}-r|)$ the single layer potential can be written as

$$Su=2\int_{\partial D} G(\hat{r}-r)\frac{\partial \psi}{\partial n}(r)ds(r)=\int_0^{2\pi} M(t,\tau)\frac{\partial \psi}{\partial n}(\tau)d\tau, \tag{20}$$

where

$$M(t,\tau)=\frac{ia}{2}H_0^{(1)}(kr(t,\tau)), \tag{21}$$

$$r(t,\tau)=2a\left|\sin(\frac{\tau-t}{2})\right|. \tag{22}$$

Since M has a logarithmic singularity when $t=\tau$, it has to be extracted out of M using the power series expansion for the second kind bessel function with zeroth order Y_0 [2], namely

$$Y_0(z) = \frac{2}{\pi}\ln\frac{z}{2}J_0(z) + C\frac{2}{\pi}J_0(z) - \frac{2}{\pi}\sum_{k=1}^{\infty} a_k \frac{(-1)^k}{(k!)^2}\left(\frac{z}{2}\right)^{2k}, \tag{23}$$

where

$$a_k = \sum_{m=1}^{k}\frac{1}{m}, \tag{24}$$

$$C = \lim_{p\to\infty}\left(\sum_{m=1}^{p}\frac{1}{m} - \ln p\right). \tag{25}$$

Therefore, M can be rewritten as

$$M(t,\tau) = \frac{ia}{2}H_0^{(1)}(kr(t,\tau)) \tag{26}$$

$$= \frac{ia}{2}(J_0(kr(t,\tau)) + iY_0(kr(t,\tau))) \tag{27}$$

$$= \frac{ia}{2}J_0(kr(t,\tau)) - \frac{a}{2}Y_0(kr(t,\tau)) \tag{28}$$

$$= \frac{ia}{2}J_0(kr(t,\tau)) - \frac{a}{2}\left(\frac{2}{\pi}\ln\frac{kr(t,\tau)}{2}J_0(kr(t,\tau))\right.$$
$$\left. + C\frac{2}{\pi}J_0(kr(t,\tau)) - \frac{2}{\pi}\sum_{k=1}^{\infty} a_k\frac{(-1)^k}{(k!)^2}\left(\frac{kr}{2}\right)^{2k}\right). \tag{29}$$

Separating the natural logarithmic term yields

$$M(t,\tau) = \ln\left(4a^2\sin^2\left(\frac{t-\tau}{2}\right)\right)M_1(t,\tau) + M_2(t,\tau), \tag{30}$$

where

$$M_1(t,\tau) = -\frac{a}{2\pi}J_0(kr(t,\tau)), \tag{31}$$

$$M_2(t,\tau) = \frac{ia}{2}J_0(kr) - C\frac{a}{\pi}J_0(kr) + \frac{a}{\pi}\sum_{k=1}^{\infty} a_k\frac{(-1)^k}{(k!)^2}\left(\frac{kr}{2}\right)^{2k}$$
$$-\frac{a}{\pi}\ln\frac{k}{2}J_0(kr) \tag{32}$$

$$= M(t,\tau) - \ln\left(4a^2\sin^2\left(\frac{t-\tau}{2}\right)\right)M_1(t,\tau). \tag{33}$$

Now $M_1(t,\tau)$ and $M_2(t,\tau)$ are both analytic and the diagonal term of $M_2(t,\tau)$ can be obtained from (32) by setting $\tau = t$

$$M_2(t,t) = \frac{ia}{2} - \frac{a}{\pi}\ln\frac{k}{2} - C\frac{a}{\pi}. \tag{34}$$

Finally, a quadrature rule can be used to discretize the integral

$$2\int_{\partial D} G(\hat{r}-r)\frac{\partial\psi}{\partial n}ds = \int_0^{2\pi} M(t,\tau)\frac{\partial\psi}{\partial n}(\tau)d\tau \tag{35}$$

$$= \int_0^{2\pi}\left\{\ln\left(4a^2\sin^2\left(\frac{t-\tau}{2}\right)\right)M_1(t,\tau) + M_2(t,\tau)\right\}\frac{\partial\psi}{\partial n}(\tau)d\tau \tag{36}$$

$$= \int_0^{2\pi}\left\{\ln\left(4\sin^2\left(\frac{t-\tau}{2}\right)\right)M_1(t,\tau) + \ln(a^2)M_1(t,\tau) + M_2(t,\tau)\right\}$$
$$\times\frac{\partial\psi}{\partial n}(\tau)d\tau \tag{37}$$

$$\approx \sum_{j=1}^{2n-1} R_j^n(t)M_1(t,t_j)\frac{\partial\psi}{\partial n}(t_j) + \frac{\pi}{n}\sum_{j=0}^{2n-1}\{\ln(a^2)M_1(t,t_j) + M_2(t,t_j)\}$$
$$\times\frac{\partial\psi}{\partial n}(t_j), \tag{38}$$

where

$$R_j^n(t) = -\frac{2\pi}{n}\sum_{m=1}^{n-1}\frac{1}{m}\cos m(t-t_j) - \frac{\pi}{n^2}\cos n(t-t_j), \tag{39}$$

$$t_j = \frac{\pi j}{n}, \quad j = 0, 1, 2, \ldots, 2n-1. \tag{40}$$

We used special weight (39) for the natural logarithm part for the quadrature [6]. For the remaining part, trapezoidal rules are used. Other method for handling the singularities can be found in [7].

3.2. Double Layer Potential (D)

Double layer potential can be rewritten in a parametric form on a circular domain as

$$Du = 2\int_{\partial D}\frac{\partial G}{\partial n}(\hat{r}-r)\psi(r)ds(r) = \int_0^{2\pi} L(t,\tau)\psi(\tau)d\tau, \tag{41}$$

where

$$L(t,\tau) = -\frac{ik}{4} H_1^{(1)}(kr(t,\tau)) r(t,\tau). \tag{42}$$

Again, similar calculation as for single layer potential

$$L(t,\tau) = \ln\left(4a^2 \sin^2 \frac{t-\tau}{2}\right) L_1(t,\tau) + L_2(t,\tau), \tag{43}$$

where

$$L_1(t,\tau) = \frac{k}{4\pi} J_1(kr(t,\tau)) r(t,\tau), \tag{44}$$

$$L_2(t,\tau) = L(t,\tau) - L_1(t,\tau) \ln\left(4a^2 \sin^2 \frac{t-\tau}{2}\right), \tag{45}$$

$$r(t,\tau) = 2a \left|\sin\left(\frac{\tau - t}{2}\right)\right|. \tag{46}$$

Also, the diagonal term of L_2 can be deduced from

$$\lim_{z\to\infty} z H_1^{(1)}(z) = \frac{2}{i\pi}. \tag{47}$$

Thus,

$$L_2(t,t) = -\frac{1}{2\pi}. \tag{48}$$

Finally, we have

$$2\int_{\partial D} \frac{\partial G}{\partial n}(\hat{r} - r)\psi(r)ds = \int_0^{2\pi} L(t,\tau)\psi(\tau)d\tau \tag{49}$$

$$= \int_0^{2\pi} \left\{\ln\left(4a^2 \sin^2\left(\frac{t-\tau}{2}\right)\right) L_1(t,\tau) + L_2(t,\tau)\right\} \frac{\partial \psi}{\partial n} d\tau \tag{50}$$

$$= \int_0^{2\pi} \left\{\ln\left(4\sin^2\left(\frac{t-\tau}{2}\right)\right) L_1(t,\tau) + \ln(a^2) L_1(t,\tau) + L_2(t,\tau)\right\} \times \frac{\partial \psi}{\partial n}(\tau) d\tau \tag{51}$$

$$\approx \sum_{j=1}^{2n-1} R_j^n(t) L_1(t,t_j) \frac{\partial \psi}{\partial n}(t_j) + \frac{\pi}{n} \sum_{j=0}^{2n-1} \{\ln(a^2) L_1(t,t_j) + L_2(t,t_j)\} \times \frac{\partial \psi}{\partial n}(t_j), \tag{52}$$

where

$$R_j^n(t) = -\frac{2\pi}{n}\sum_{m=1}^{n-1}\frac{1}{m}\cos m(t-t_j) - \frac{\pi}{n^2}\cos n(t-t_j), \tag{53}$$

$$t_j = \frac{\pi j}{n}, \quad j = 0, 1, 2, \ldots, 2n-1. \tag{54}$$

3.3. Mode Searching

Using the method described in previous section, operator equation can be discretized into the matrix equation. The secant method [5] is employed to find zeros of $f(\beta) := |det(A(\beta))|$, namely

$$\beta_{i+1} = \beta_i - \frac{f(\beta_i)(\beta_i - \beta_{i-1})}{f(\beta_i) - f(\beta_{i-1})}. \tag{55}$$

In order to use secant method, we need a good initial guess to have the numerical convergence. To determine the initial guess, we graphed the determinant over certain ranges and approximated the local minima (See the Fig. 2). The Range of the search can be determined by the refractive

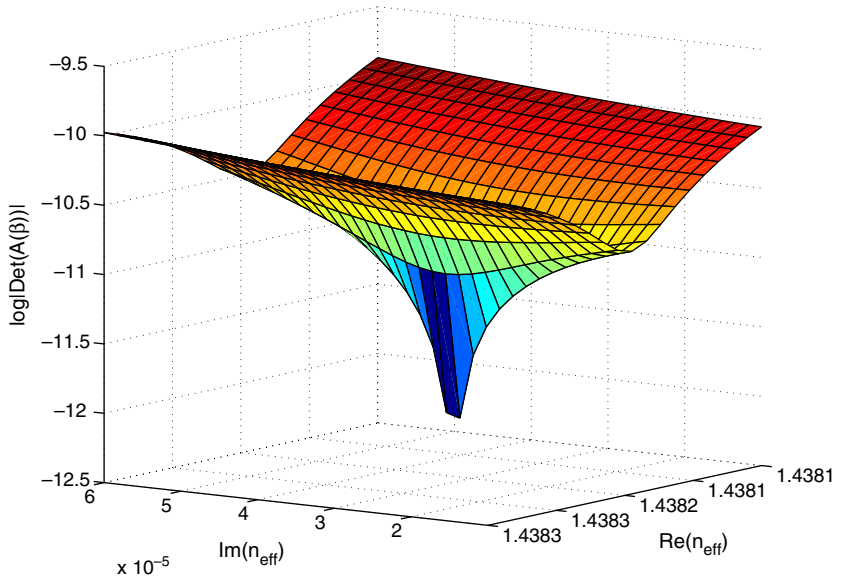

Fig. 2. Determinant of matrix on the complex plane $n_1 = 1.44$, $n_2 = 1.8$, $d = 3.315\,\mu m$, $\lambda = 0.815\,\mu m$, and $\Lambda = 5.64\,\mu m$.

index of the material used in the PCF. In the case of an air-silica fiber, effective refractive index is less than the refractive index of silica and greater than that of the air, and effective refractive index is less than the lower refractive index in the case of a photonic bandgap fiber (PBF). The main drawback of using the secant method is that a real initial guess will only converge to a real number, although Müller method (another variation of the Newton method) can be used to find a complex root regardless of the initial condition. Thus, in order to use secant method to find the complex propagation constant β, initial guess must be a complex number.

4. NUMERICAL RESULTS

In this section we calculate the propagation characteristics of two different PCFs using the BIE to validate our method. Unless otherwise stated in the paper, the PCFs we used in our simulation contain only the nearest layer of holes in order to minimize the computation time.

4.1. Air-silica Fiber

In an air-silica fiber, holes remain empty with refractive index equal to one [3]. The average refractive index is therefore lower than that of the core, and light is guided through total internal reflection. Figure 3 depicts the intensity profile of the fundamental mode calculated at $\lambda = 1.5\,\mu m$ for a PCF with $d = 2.0\,\mu m$ and $\Lambda = 3.0\,\mu m$. Clearly a well-confined mode is obtained. Figure 4 shows both the real and imaginary parts of the effective refractive index $n_{\text{eff}} = \beta/k_0$ of the fundamental mode as a function of propagation wavelength λ between 0.9 and $1.7\,\mu$m for a PCF with $d = 2.26\,\mu$m and $\Lambda = 4\,\mu$m. As shown, the real part of n_{eff} decreases with increasing wavelength, indicating the dispersion is dominated by material response (silica). On the other hand, the imaginary part of n_{eff} increases with increasing wavelengths, indicating the confinement becomes weaker as more light penetrates through the holes, and therefore leaks out.

To address the effectiveness of light confinement in the core by the surrounding holes, Fig. 5 shows the imaginary part of n_{eff} as a function of number of layers of holes. As indicated, the imaginary part of n_{eff} decreases exponentially with increasing number of layers of holes, suggesting that more than one layer of holes is desired to reduce the confinement loss.

4.2. Photonic Bandgap Fiber

In a PBF, the average refractive index of the cladding is larger than that of the core, which can be realized either by a large air core

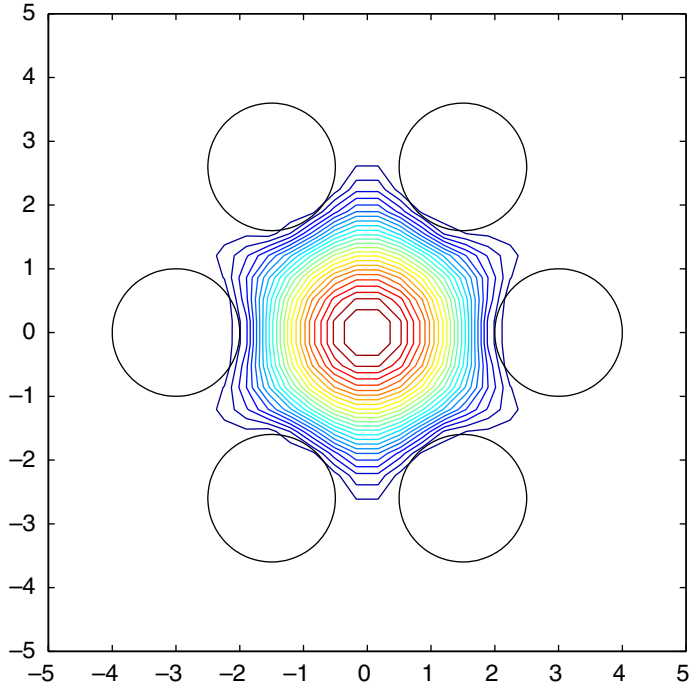

Fig. 3. Contour plot of intensity field with $n_1 = 1.45$, $n_2 = 1.0$, $d = 2.0\,\mu m$, $\lambda = 1.5\,\mu m$, and $\Lambda = 3.0\,\mu m$.

surrounded by a array of smaller air holes [8] or by filling the holes in air-silica fibers with liquid whose refractive index is larger than that of the silica [4]. In this configuration, light is confined in the core when it falls into the stop band of the cladding. Reference [1] shows, when the periodicity of holes is much larger than the wavelength of light and the index contrast between core and holes is large, the light confinement is achieved based on so-called antiresonant reflecting optical waveguide (ARROW) model [9] rather than the otherwise well-known Bragg resonance [8]. According to the ARROW model, the light is confined in the core when it is reflected off the Fabry–Perot resonator formed by the high-indexed holes. If the wavelength of light matches the resonance condition of the Fabry–Perot resonator [12]:

$$\lambda_m = \frac{2d\sqrt{n_2^2 - n_1^2}}{m + 1/2}, \quad m = 1, 2, \ldots . \tag{56}$$

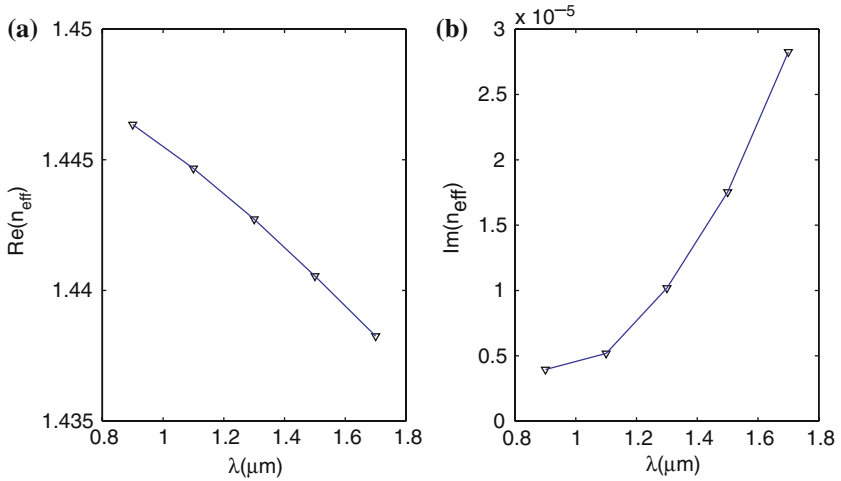

Fig. 4. (a) Real and (b) imaginary part of n_{eff} for the one layer with $n_1 = 1.45$, $n_2 = 1.0$, $d = 2.26\,\mu m$, and $\Lambda = 4.0\,\mu m$. Lines are connected between dots for eye-guide purpose only.

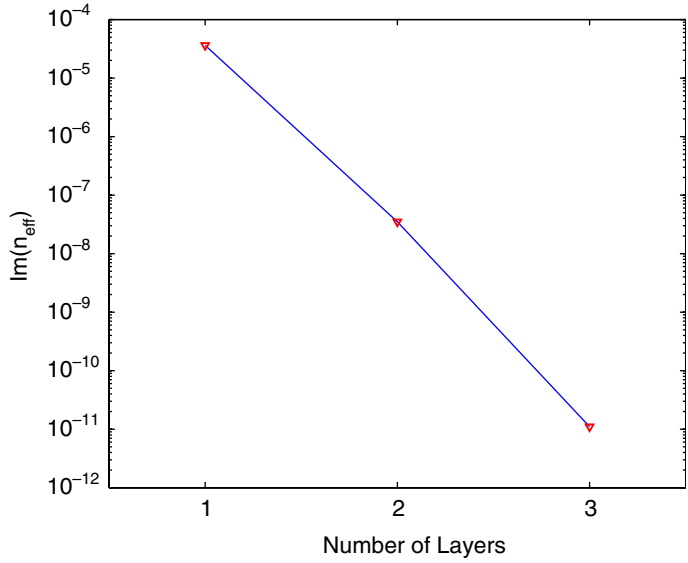

Fig. 5. Loss as a function of number of layers with $n_1 = 1.45$, $n_2 = 1.0$, $d = 1.61\,\mu m$, $\lambda = 1.55\,\mu m$, and $\Lambda = 2.3\,\mu m$. Lines are connected between dots for eye-guide purpose only.

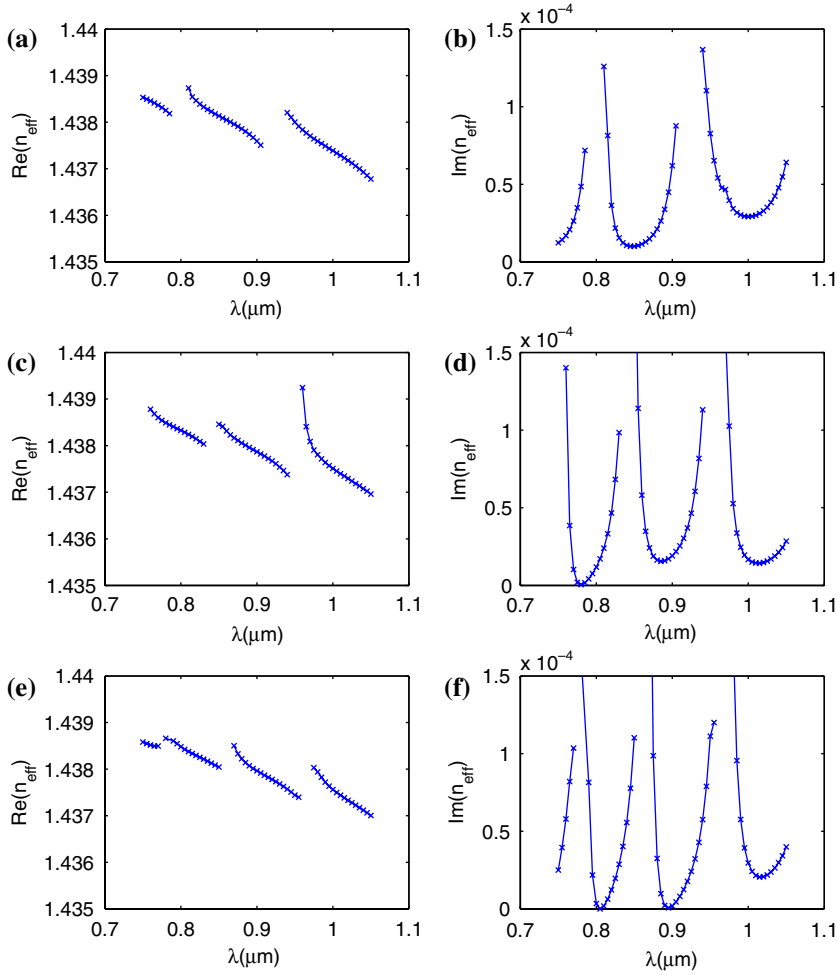

Fig. 6. Real(left) and imaginary(right) part of n_{eff} for the one layer with $n_1 = 1.44$, $d = 3.315\,\mu m$, $\Lambda = 5.64\,\mu m$, (a),(b) $n_2 = 1.7$, (c),(d) $n_2 = 1.8$, and (e),(f) $n_2 = 1.9$. Lines are connected between dots for eye-guide purpose only.

then, light transmits through such resonators and hence leaks out of the core. In this section, we apply the BIE method to calculate the propagation characteristics of PBF where the ARROW model is applicable. The PBF we used for the calculation has $d = 3.315\,\mu m$, $\Lambda = 5.640\,\mu m$, and refractive index of silica $n_1 = 1.44$. Figure 6 compares the wavelength dependence of the real and imaginary parts of n_{eff} of PBFs for refractive index of holes $n_2 = 1.7$, 1.8, and 1.9, respectively. As shown,

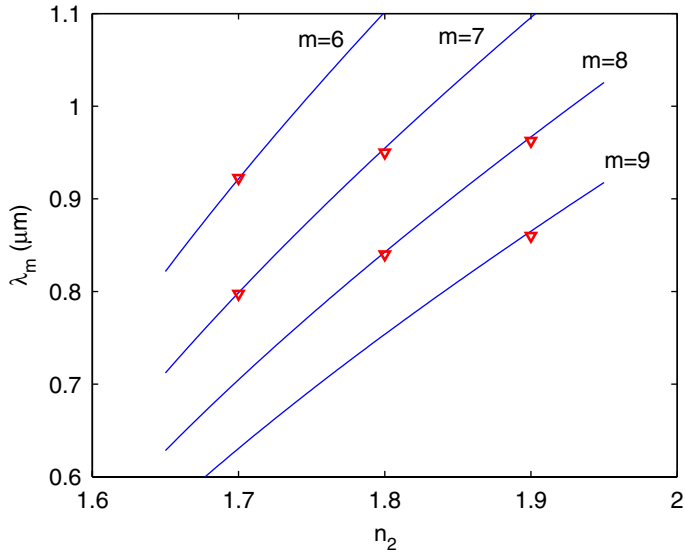

Fig. 7. Dependence of resonance frequency on refractive index n_2 in PBFs calculated using BIE method (triangle) and from Eq. (56) (solid line).

both the real and imaginary parts of n_{eff} exhibit peaks corresponding to Fabry-Perot-type resonances. In addition to the resonances, the real part of n_{eff} has a background that monotonically levels off as wavelength increases, a trend consistent with the air-silica PCF (Figure 4(a)) and is a consequence of material dispersion of silica. Similarly, the imaginary part of n_{eff} has a baseline that monotonically increases as wavelength increases, a trend consistent with the air-silica PCF (Figure 4(b)) and is a consequence of weaker confinement at large wavelength.

Figure 7 summaries the resonance frequencies obtained from Fig. 6 by averaging the last point on the left of the resonance and the first point on the right of the resonance. Also displayed is the theoretical curves calculated from Eq. (56). Excellent agreement is obtained.

5. CONCLUSION

A BIE for PCF is formulated, which based on Huygen's principal and Green's function. Due to the nature of its formulation, the BIE method can handle almost arbitrary lattice configurations, such as shapes, locations, and refractive index of holes. In this paper we have applied the BIE method to calculate the real and imaginary parts of the propagation constant for both air-silica fiber and PBF, and these results agree well with those obtained

by other methods. We are applying this method to other more complicated novel fiber structures such as hollow core PCF, Double-clad PCF.

REFERENCES

1. Abeeluck, A. K., Litchinitser, N. M., Headley, C., and Eggleton, B. J. (2002). Analysis of spectral characteristics of photonic bandgap waveguides. *Opt. Exp*. **10**(23), 1320–1333.
2. Abramowitz, M., and Stegun, I. A. (1970). *Handbook of Mathematical Functions*, Dover.
3. Birks, T. A., Knight, J. C., and Russell, P. St. J. (1997). Endless single-mode photonic crystal fiber. *Opt. Lett.* **22**, 961–963.
4. Bise, R. T., Windeler, R. S., Kranz, K. S., Kerbage, C., Eggleton, B. J., and Trevor, D. J. (2002). Tunable photonic band gap fiber. In *Optical Fiber Communication Conference, Vol. 70 of OSA Trends in Optics and Photonics Series, Optical Society of America*, Washington, D.C., pp. 466–468.
5. Burden, R. L., and Faires, J. D. (2000). *Numerical Analysis*, Brooks Cole.
6. Colton, D., and Kress, R. (1997). *Inverse Acoustic and Electromagnetic Scattering Theory*, 2nd edn., Springer.
7. Chen, Q.-Y., Tang, T., Teng, Z.-H. (2004). A fast numerical method for integral equations of the first kind with logarithmic kernel using mesh grading. *J. Comput. Math.* **22**, 287–298.
8. Cregan, R. F., Mangan, B. J., Knight, J. C., Birks, T. A., Russell, P. St. J., Roberts, P. J., and Allan, D. C. (1999). Single-mode photonic band gap guidance of light in air. *Science* **285**(3), 1537–1539.
9. Duguay, M. A., Kokubun, Y., and Koch, T. L. (1986). Antiresonant reflecting optical waveguides in SiO_2-Si multilayer structures. *Appl. Phys. Lett.* **49**(1), 13–15.
10. Fini, J. M. (2003). Analysis of microstructure optical fibers by radial scattering decomposition. *Opt. Lett.* **28**(12), 992–994.
11. Knight, J. C. (2003). Photonic crystal fibres. *Nature* **424**, 847–851.
12. Litchinitser, N. M., Dunn, S. C., Steinvurzel, P. E., Eggleton, B. J., White, T. P., Mcphedran, R. C., and Martijn de Sterke, C. (2004). Application of an ARROW model for designing tunable photonic devies. *Opt. Exp.* **12**(8), 1540–1550.
13. Nédélec, J.-C. (2001). *Acoustic and Electromagnetic Equations, Integral Representations for Harmonic Problem*, Springer.
14. Russell, P. (2003). Photonic crystal fibers. *Science* **299**, 358–362.
15. Saitoh, K., and Koshiba, M., (2002). Full-vectorial imaginary-distance beam propagation method based on a finite element scheme: application to photonic crystal fibers. *IEEE J. Quantum Electron.* **38**(7), 927–933.
16. Venakides, S., Haider, M. A., and Papanicolaou, V. (2000). Boundary integral calculations of two dimensional electromagnetic scattering by phtonic crystal Fabry–Perot structures. *SIAM J. Appl. Math.* **60**(5), 1686–1706.
17. Wang, X., Lou, J., Lu, C., and Zhao, C.-L. (2004). Modeling of PCF with multiple reciprocity boundary element method. *Opt. Exp.* **12**(5), 961–966.
18. White, T. P., Mcphedran, R. C., de Sterke, C. M., Botten, L. C., and Steel, M. J. (2001). Confinement losses in microstructured optical fiber. *Opt. Lett.* **26**(21), 1660–1662.
19. White, T. P., Mcphedran, R. C., de Sterke, C.M., Litchinitser, N. M., and Eggleton, B. J. (2002). Resonance and Scattering in microstructured optical fibers. *Opt. Lett.* **27**(22), 1977–1979.